Phases and collective modes of bosons in a triangular lattice at finite temperature: A cluster mean field study

M. Malakar,[1] S. Ray ●,[2] S. Sinha,[1] and D. Angom ●[3]

[1]*Indian Institute of Science Education and Research Kolkata, Mohanpur, Nadia 741246, India*
[2]*Department of Chemistry, Ben-Gurion University of the Negev, Beer-Sheva 84105, Israel*
[3]*Physical Research Laboratory, Ahmedabad 380009, Gujarat, India*

Motivated by the realization of Bose-Einstein condensates in noncubic lattices [J. Struck *et al.*, Science **333**, 996 (2011)], in this work we study the phases and collective excitation of bosons with nearest-neighbor interaction in a triangular lattice at finite temperature, using mean field (MF) and cluster mean field (CMF) theory. We compute the finite-temperature phase diagram both for hardcore and softcore bosons, as well analyze the effect of correlation arising due to geometric frustration of a triangular lattice and interaction systematically using the CMF method. A semianalytic estimate of the transition temperatures between different phases is derived within the framework of MF Landau theory, particularly for hardcore bosons. Apart from the usual phases such as density waves and superfluid, we also characterize different supersolids. These phases and their transitions at finite temperature are identified from the collective modes. The low-lying excitations, particularly Goldstone and Higgs modes of the supersolid, can be detected in the ongoing cold atom experiments.

I. INTRODUCTION

Frustrated lattice systems are one of the most active research areas of condensed matter physics, which has led to the observation of various exotic phases of matter [1] such as spin liquids [2], the spin ice state in pyrochlore material [3,4], as well magnetic phases and phase transition [5,6]. In recent experiments, antiferromagnetic spin models in a triangular lattice have been realized in complex compounds such as $Ba_3CoSb_2O_9$, and its magnetization process, specific heat, as well as the collective excitation are also measured [7–9]. The realization of Bose-Einstein condensates (BECs) in noncubic lattice geometries, e.g., experimental demonstration of the superfluid-Mott insulator (SF-MI) transition in triangular and hexagonal optical lattices [10], has further opened up the possibility to explore the competition between interaction and geometric frustration. Ultracold bosonic atoms trapped in a triangular optical lattice have further paved the way to study different magnetic phases of frustrated classical spin models [11] and in the presence of a synthetic gauge field [12]. The existence of different types of supersolid phases, and their melting driven by either quantum or thermal fluctuation in triangular lattices, have been theoretically investigated [13–17].

Supersolid is a state of matter where particles are organized in a crystalline order, and they show a dissipation-less superflow [18–20]. Such a phase of matter has been predicted in a number of theoretical studies over the years, particularly in bosonic systems with long range interaction in optical lattices [21–26], Josephson junction arrays [27,28], in a Bose-Fermi mixture [29–31], and so on. As a result of experimental progress in ultracold atomic systems, quantum gases with dipolar interaction [32,33], spin-orbit coupled condensate [34], and Rydberg gases [35–37] have become promising candidates to search for the supersolid phase. In recent cold-atom experiments, supersolid has been observed in spin-orbit coupled Bose-Einstein condensates (BECs) [38], BECs in an optical lattice [39] and coupled to an optical cavity [40], and trapped dipolar BECs of erbium (Er) and dysprosium (Dy) atoms [41–43]. Apart from the density modulation revealing the crystalline order, the signature of $U(1)$ symmetry breaking has also been confirmed experimentally from low-energy collective excitation such as Goldstone and Higgs modes [40–43].

On the other hand, a stable supersolid formation due to the competition between particle interaction and frustration in a triangular lattice has been predicted in a number of theoretical studies [13–17,44–48]. A supersolid phase of Rydberg excited atoms in a triangular lattice has also been predicted [49]. At finite temperature, the equilibrium phases of hardcore bosons in a triangular lattice have been studied [17]. The superfluid to Mott insulator transition at finite temperatures in a cubic lattice has also been investigated theoretically [50–54]. However, a systematic analysis to understand the interplay between the geometric frustration of a lattice and interaction, leading to different density ordering at finite temperature and characterization of such phases from collective excitations, is beyond the scope of these studies. Motivated by recent experiments, in this work we primarily chart out the phases of bosons in a triangular lattice at finite temperature using the cluster mean field (CMF) technique, and we compute the collective excitation for both of the following cases: one with on-site hardcore repulsion, i.e., $U \to \infty$, and another with finite U, which is a more realistic scenario. We supplement semianalytical results obtained from the Landau-Ginzburg

theory, which qualitatively captures the numerically observed phases of hardcore bosons at finite temperature. The transition between these phases is captured from the collective modes that can be detected in cold atom experiments.

The paper is organized as follows. In Sec. II we describe the Bose-Hubbard model on a triangular lattice, and we demonstrate the cluster mean field method extended to finite temperature. In Sec. III A we provide the mean field phase diagram of hardcore bosons followed by the semianalytic estimate of the transition temperature from Landau-Ginzburg theory. The linear stability of these phases is analyzed, and their collective excitation is computed in Sec. III B. The effect of correlation is discussed using the cluster mean field in Sec. III C, and the results are compared with the existing quantum Monte Carlo (QMC) studies. In Sec. IV we discuss the zero and finite temperature phases of bosons with finite on-site repulsion, and we compute their collective modes. Finally, we summarize our work and conclude in Sec. V.

II. MODEL AND STATE-OF-THE-ART METHOD

The Bose-Hubbard model with nearest neighbor interaction in the grand canonical ensemble can be described in general by the Hamiltonian

$$\hat{H} = -t \sum_{\langle i,j \rangle} (\hat{a}_i^\dagger \hat{a}_j + \text{H.c.}) - \mu \sum_i \hat{n}_i + V \sum_{\langle i,j \rangle} \hat{n}_i \hat{n}_j$$
$$+ \frac{U}{2} \sum_i \hat{n}_i (\hat{n}_i - 1), \tag{1}$$

where, $\hat{a}_i^\dagger$ ($\hat{a}_i$) are the bosonic creation (annihilation) operator at the ith site, $\hat{n}_i$ represents the local number operator, t and V are the hopping amplitude and interaction strength, respectively, between the nearest-neighbor sites of the triangular lattice denoted by $\langle i, j \rangle$, U is the on-site interaction, and μ is the chemical potential. In what follows, we set $\hbar = 1$, Boltzmann constant $k_B = 1$, and measure all the energies in the unit of interaction strength V unless it is otherwise mentioned.

We focus on the equilibrium phases of the above model at a finite temperature T using the cluster mean field (CMF) method. Such a method has been used previously to study zero temperature phases and nonequilibrium dynamics of bosons in an optical lattice [47,55–57]. We extend this to finite temperature and study the effect of correlation by considering a cluster $\mathcal{C}$ of different sizes in a triangular lattice as illustrated in Fig. 1. While all the correlations are considered exactly within the cluster $\mathcal{C}$ of a given size using exact diagonalization, the interaction and hopping between edge sites of $\mathcal{C}$ and its neighboring sites outside $\mathcal{C}$ are treated at the mean field level. More generically, the composite Hamiltonian can be written as

$$\hat{H} = \hat{H}_{\mathcal{C}} + \hat{H}_{\text{MF}}, \tag{2}$$

where $\hat{H}_{\mathcal{C}}$ describes the bosons within the cluster, and the mean field term corresponding to the edge sites can be written as

$$\hat{H}_{\text{MF}} = \sum_{i \in \text{edge sites}} \hat{H}_{\text{MF}}^i,$$

$$\hat{H}_{\text{MF}}^i = \sum_{\langle i,j \rangle, \, j \notin \mathcal{C}} [-t(\alpha_j \hat{a}_i^\dagger + \alpha_j^* \hat{a}_i) + V n_j \hat{n}_i]. \tag{3}$$
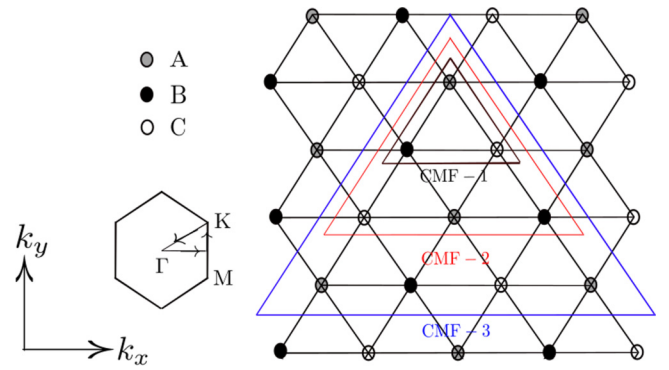

FIG. 1. Schematic representation of the triangular lattice and its three-sublattice structure. The reduced hexagonal Brillouin zone is shown on the left. The arrows indicate the lines along which collective modes of the phases are calculated in the subsequent sections. The different sized clusters used in the cluster mean field are shown by the enclosing triangles on the right.

Exploiting the sublattice symmetry throughout the lattice, the mean field values α_j and n_j can be obtained from $\langle \hat{a}_{A,B,C} \rangle$ and $\langle \hat{n}_{A,B,C} \rangle$, respectively, where the sublattices A, B, and C belong to the cluster $\mathcal{C}$. Note that in the case of zero temperature, the average of observable is denoted by $\langle \cdot \rangle \equiv \langle \psi | \cdot | \psi \rangle$, $|\psi\rangle$ being the ground state of $\hat{H}$. At a finite temperature, this amounts to a thermal average, $\langle \cdot \rangle \equiv \text{Tr}(\hat{\rho}_T \cdot)$, where the thermal density matrix is given by

$$\hat{\rho}_T = \frac{e^{-\beta \hat{H}}}{Z}, \quad Z = \text{Tr}(e^{-\beta \hat{H}}), \quad \beta = 1/T. \tag{4}$$

Solving the mean field self-consistency, we finally obtain the equilibrium density matrix $\hat{\rho}_T$ at a finite temperature T with converged free energy $F = E - TS$, where $E = \langle \hat{H} \rangle$ and von Neumann entropy $S = -\text{Tr}(\hat{\rho}_T \ln \hat{\rho}_T)$. Different physical quantities at finite temperature can be obtained by averaging over the cluster using the density matrix $\hat{\rho}_T$.

III. PHASES AND COLLECTIVE EXCITATION OF HARDCORE BOSON

In this section, we discuss the phases and collective modes of bosons in a triangular lattice with hardcore repulsion, i.e., $U \to \infty$ allowing not more than one boson per site. First we present the phase diagram using standard mean field calculation and subsequently show how the results get improved by introducing clusters and thereby incorporating correlations in the system.

A. Mean field phase diagram

We consider one unit cell consisting of three sublattices A, B, and C, which are decoupled at the mean field level. Therefore, the total density matrix of a unit cell in a triangular lattice can be written as

$$\hat{\rho}_T = \prod_i \hat{\rho}_i, \quad \hat{\rho}_i = \begin{bmatrix} \frac{1}{2}(1 - m_i) & \alpha_i^* \\ \alpha_i & \frac{1}{2}(1 + m_i) \end{bmatrix}, \tag{5}$$

where $\hat{\rho}_i$, $i \in \{A, B, C\}$ represents a thermal density matrix satisfying $\text{Tr}[\hat{\rho}_i] = 1$. It can be noted that by definition, the
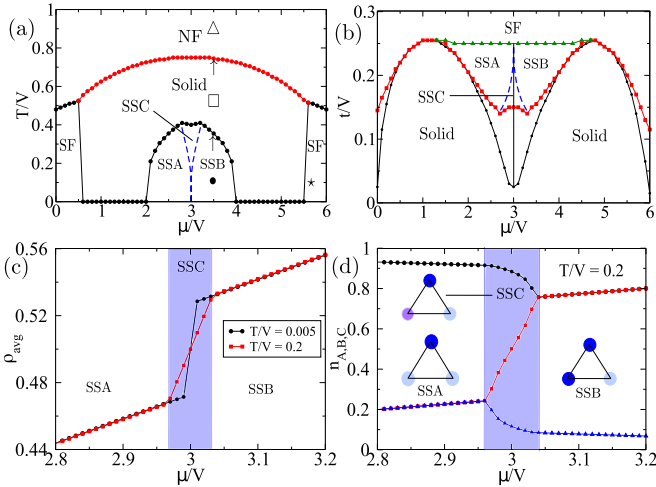
FIG. 2. Finite temperature mean field phase diagram of hardcore bosons in a triangular lattice: (a) in μ vs T plane for $t = 0.2$, and (b) in μ vs t plane for different temperatures $T = 0.005$ (black solid lines with circles) and $T = 0.2$ (red solid lines with squares). The region of supersolid SSC appearing only at higher temperature $T = 0.2$ is separated by dashed lines. (c) Average density $\rho_{\mathrm{avg}} = \sum_i n_i/3$, and (d) sublattice densities $n_{\mathrm{A,B,C}}$ are plotted as a function of μ for temperatures specified in the inset. Collective excitation at the points marked by bullets in (a) is shown in Fig. 3. Vanishing of respective order parameters and the excitation energy gap at the SS-solid and solid-NF boundary (marked by $\uparrow$) are depicted in Fig. 4. Throughout the manuscript, we use dimensionless energy e.g. hopping $t \equiv t/V$, temperature $T \equiv T/V$ (Boltzmann constant $k_B = 1$) unless the scaling is explicitly mentioned.

local SF order parameter is $\langle \hat{a}_i \rangle = \alpha_i$, and m_i is related to the local density as $\langle \hat{n}_i \rangle = (1 + m_i)/2$. Thus the corresponding mean field free energy at temperature T for a given site can be written as

$$F_{\mathrm{MF}}^i = -\frac{3t}{2}\left(\alpha_i^* \sum_{\bar{i} \neq i} \alpha_{\bar{i}} + \alpha_i \sum_{\bar{i} \neq i} \alpha_{\bar{i}}^*\right) - \frac{\mu}{2}(1 + m_i)$$
$$+ \frac{3V}{8}(1 + m_i) \sum_{\bar{i} \neq i}(1 + m_{\bar{i}}) - TS_i, \qquad (6)$$

where i and $\bar{i}$ denote nearest neighbor sites $\in \{A, B, C\}$, and the von Neumann entropy S_i is given by

$$S_i = -\sum_{\sigma = +,-} \lambda_\sigma^i \ln \lambda_\sigma^i, \quad \lambda_\pm^i = \frac{1 \pm \sqrt{m_i^2 + 4|\alpha_i|^2}}{2}. \qquad (7)$$

Minimizing the average free energy $F = \sum_i F_{\mathrm{MF}}^i/3$ with respect to the order parameters α_i's and m_i's, we obtain the phase diagram in the μ versus T plane for a fixed tunneling amplitude t as shown in Fig. 2(a). At low temperature, apart from homogeneous superfluid, two types of density waves exist, which at $T = 0$ have a sublattice density structure $(1,0,0)$ and $(1,1,0)$ for $\mu < 3$ and $\mu > 3$, respectively; as t is increased, they melt to form hole and particle dominated supersolids, namely SSA and SSB for $\mu \lesssim 3$ [13,14]. At finite T, these two solid lobes and the supersolid are shown in Fig. 2(b). It can be noted from Fig. 2(c) that, as $T \to 0$, the

transition between SSA and SSB phases at $\mu = 3$ is associated with a jump in average density (also in average SF order parameter) as shown by the vertical dashed and solid lines in Figs. 2(a) and 2(b), respectively. However, within MF we find that such an abrupt jump is smeared out at finite temperature by the appearance of another supersolid phase, which we call SSC [see Fig. 2(c)]. The sublattice density structure of SSC is $n_A \neq n_B \neq n_C$, which is shown in Fig. 2(d). Such a supersolid phase appears between SSA and SSB at higher T as marked by the dashed lines in Figs. 2(a) and 2(b). Moreover, we observe a kink in the SS-solid boundary for $\mu \sim 2.8$–3.2 in Fig. 2(a), and these kinks correspond to the end of the second-order line between SSA/SSB and SSC. As temperature is lowered and in the limit $T \to 0$, the phase boundaries agree with the zero temperature mean field phase diagram [13].

Next we focus on the transitions between different phases with increasing temperature. We observe the transition from (i) superfluid (SF) to normal fluid (NF), (ii) density wave (DW)/solid to NF, and (iii) melting of supersolid (SS) to NF in two steps via a DW/solid phase. The nature of the transition and an estimate of the corresponding critical temperature can be obtained by expanding the free energy F with respect to the appropriate order parameter ϕ and rewriting it in the so called Landau-Ginzburg (LG) form

$$F(\phi) = a + b\phi + c\phi^2 + d\phi^3 + e\phi^4 + \cdots, \qquad (8)$$

where the coefficients $a, b, c, \ldots$ depend on the values of the parameters t, μ, and T. In the homogeneous phase, the SF to NF transition can be captured from the vanishing of SF order parameter $\phi \equiv |\alpha|$. Near the transition, the free energy F can be expanded in even powers of $|\alpha|$ and the order parameter vanishes continuously at the critical temperature. The continuous transition from SF-NF and estimation of the critical temperature from the LG free energy are discussed in Appendix A. In the DW/solid phase, the SF order parameter vanishes and density ordering takes the form $n_A = n_B \neq n_C$. At finite temperature, there is another type of solid that also appears near the SSC-solid boundary around $\mu = 3$, which has a similar sublattice density structure to that in SSC. For the solid to NF transition, the sublattice density difference $n_{A,B} - n_C = \delta$ plays the role of an order parameter, and the free energy contains both even and odd powers of δ. Such MF free energy yields a first-order transition similar to the three-state Pott's model [17,58] exhibiting a jump in density difference δ except at $\mu = 3$, as also discussed in Appendix A.

Next we focus on the melting of supersolid with increasing temperature. First, the SS phase melts to a solid where the SF order parameter (α) vanishes continuously at the SS-solid phase boundary [see Fig. 4(a)]. Further increase of temperature leads to the melting of the solid, and the sublattice density imbalance (δ) jumps to zero at the solid-NF boundary, as depicted in Fig. 4(b). This is atypical of a first-order transition. As can be noted from Fig. 2(a), with increasing temperature the supersolid region shrinks, and instead of a first-order line, the transition from SSA to SSB phase occurs continuously via SSC phase. Also, the two DW/solid lobes gradually merge with each other with increasing T. Such a behavior of the supersolid phase is summarized in the μ versus t phase diagram at different temperatures depicted in Fig. 2(b).

Although a first-order transition from solid to NF phase with finite T_c is observed at the MF level, the density ordering even at zero temperature cannot survive at $\mu = 3$ due to the effect of frustration. In the absence of hopping, $t = 0$, this system becomes equivalent to an antiferromagnetic Ising model with vanishing critical temperature in the absence of an external magnetic field, which corresponds to $\mu = 3$ in the present case [59–61]. Such a reduction of the critical temperature at $\mu = 3$ due to frustration cannot be captured by a simple MF method and requires more sophisticated techniques. This further motivates us to investigate the phase boundary particularly near $\mu = 3$ by incorporating correlation via the cluster mean field, which we discuss in Sec. III C. However, before going into that, we complete the mean field analysis by analyzing the collective modes of these phases at finite temperature, and we determine the MF phase boundary from the energy gap vanishing phenomena in the next section.

B. Collective modes of hardcore bosons

At the MF level, the collective excitation at zero temperature can be obtained by performing a linear stability analysis of the Gutzwiller wave function [24,36,62]. Such a method has also been extended for dissipative systems involving the fluctuations of the density matrix [63]. Here we borrow the same methodology for density matrices [63] to obtain the finite temperature excitation spectrum of lattice bosons. Within the MF approximation, the time evolution of the density matrix $\hat{\rho}_i$ at the ith site is governed by the following equation:

$$\dot{\hat{\rho}}_i = -i\big[\hat{H}_i^{\mathrm{MF}}, \hat{\rho}_i\big], \tag{9}$$

where the mean field Hamiltonian corresponding to the ith site is given by

$$\hat{H}_i^{\mathrm{MF}} = -t(\hat{a}_i^\dagger \bar{\alpha}_i + \hat{a}_i \bar{\alpha}_i^*) - \mu \hat{n}_i + V \hat{n}_i \bar{Q}_i, \tag{10}$$

where $\bar{\alpha}_i = \sum_{\langle i,j \rangle} \langle \hat{a}_j \rangle$ and $\bar{Q}_i = \sum_{\langle i,j \rangle} \langle \hat{n}_j \rangle$. Linear stability analysis can be performed by introducing small amplitude fluctuations around the steady state of the density matrix,

$$\rho_i^{a,b}(t) = \rho_{i,0}^{a,b} + \delta\rho_i^{a,b}(t), \tag{11}$$

where $\rho_{i,0}^{a,b}$ is the steady-state value of the density matrix, which satisfies $[\hat{H}_i^{\mathrm{MF}}, \hat{\rho}_{i,0}] = 0$ and corresponds to the equilibrium distribution at temperature T, and $\delta\rho_i^{a,b}$ is the fluctuation around it at the ith site. Now, plugging Eq. (11) into Eq. (9), we obtain

$$\delta\dot{\hat{\rho}}_i = -i\big[\hat{H}_i^{\mathrm{MF}}, \delta\hat{\rho}_i\big] - i\big[\delta\hat{H}_i^{\mathrm{MF}}, \hat{\rho}_{i,0}\big], \tag{12}$$

where $\delta\hat{H}_i^{\mathrm{MF}}$ contains the fluctuation in mean-field terms of $\hat{H}_i^{\mathrm{MF}}$. This is followed by substituting $\delta\rho_i^{a,b}(t) = \exp[i(kr_i + \omega t)]\delta\rho_k^{a,b}$, where $k \equiv (k_x, k_y)$ denotes the lattice momenta and r_i is the position of the ith lattice site. Retaining the linear terms in $\delta\rho_k^{a,b}$, we obtain the sets of linear equations describing the fluctuations in momentum space, and thereby construct the corresponding fluctuation matrix. For hardcore bosons, the dimension of the matrix is limited since the corresponding Fock states are restricted to 0 and 1 occupancies at each of the sublattices. It is important to mention that the
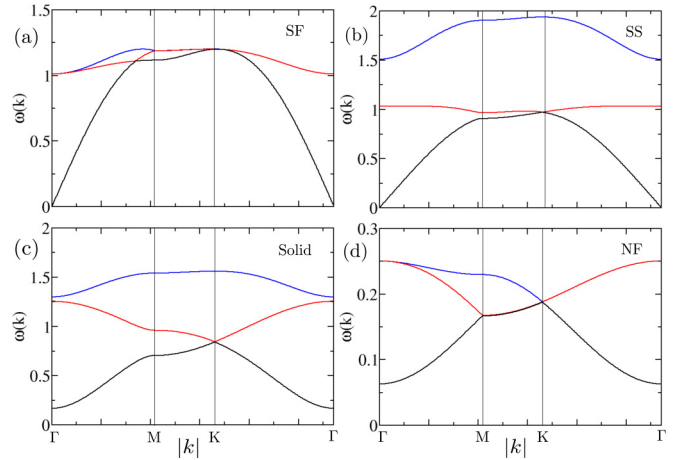

FIG. 3. (a) Collective excitation of SF phase ($\star$) at temperature $T = 0.1$ and $\mu = 5.7$. (b)–(d) Excitation spectrum of SS ($\bullet$), solid ($\square$), and NF ($\triangle$) phase at temperature $T/V = 0.1$, 0.5, and 0.9, respectively, and $\mu = 3.5$. We choose $t/V = 0.2$, and the markers indicate the location of the points in the phase diagram in Fig. 2(a). The x-values are $|k| = \sqrt{k_x^2 + k_y^2}$ in each segment along the ΓM, MK, and $K\Gamma$ lines.

fluctuations in the order parameters are induced by $\delta\rho_i(t)$, and they are included in the linearized equations. The eigenvalues $\omega(k)$ of the fluctuations yield the dispersion of the collective excitations at finite temperatures. Also, the stability of the equilibrium density matrix is ensured by the condition $\mathrm{Im}[\omega] = 0$.

At a given temperature, the steady state (equilibrium) order parameters α_i's and m_i's are obtained by minimizing F, and by substituting them in Eq. (12) we obtain six nonzero eigenvalues for each k of the form $\pm\omega(k)$. From the positive eigenvalues, we obtain three branches of excitation spectra for various phases, which are depicted in Fig. 3. Note that in the case of a homogeneous phase with translation symmetry (such as SF), these three branches correspond to a single excitation mode in an extended Brillouin zone. In what follows, we plot these collective modes $\omega(k)$ within one sublattice reduced Brillouin zone of a triangular lattice (see the schematic in Fig. 1), where Γ, M, and K represent the points $k \equiv (k_x, k_y)$ as follows [64,65]:

$$\Gamma \equiv (0,0), \quad M \equiv \left(\frac{2\pi}{3}, 0\right), \quad K \equiv \left(\frac{2\pi}{3}, \frac{2\pi}{3\sqrt{3}}\right). \tag{13}$$

From the characteristic features of the excitation modes, we identify different symmetry broken and unbroken phases and the transition between them. Both SF and SS phases are characterized by the gapless sound modes $\omega \sim c_s|k|$ for $|k| \ll 1$ due to the presence of the SF order parameter [see Figs. 3(a) and 3(b)]. This is the well known Goldstone mode corresponding to broken $U(1)$ symmetry, and it can be observed in experiment. For SS phase with broken translation symmetry, the higher energy branches of gapped excitations correspond to the optical modes in a triangular lattice [13]. On the other hand, a gap opens up for both of the insulating phases, i.e., DW and NF as shown in Figs. 3(c) and 3(d). Therefore, both the SF-NF and SS-solid transitions at finite temperature can be
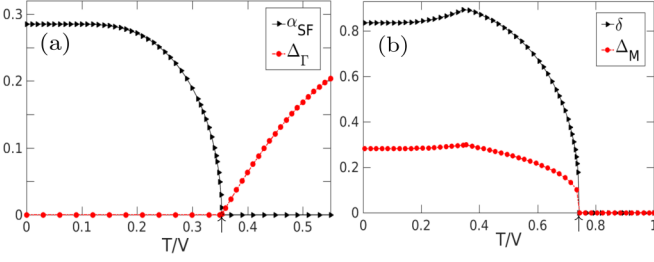
FIG. 4. (a) Energy gap opening at Γ and vanishing of average SF order parameter $\alpha_{SF} = \sum_i |\alpha_i|/3$ at SS-solid phase boundary. (b) Vanishing of sublattice density difference δ and energy gap Δ_M (at the M point) at the solid-NF transition. We set $\mu/V = 3.5$ and $t/V = 0.2$. The transition temperatures are marked on the T axis, and its location in the phase diagram is marked by ($\uparrow$) in Fig. 2(a).

identified from the energy gap opening at $|k| = 0$ (Γ point). As shown in Fig. 4(a), the SF order parameter vanishes at the critical temperature above which the energy gap increases continuously. It can be noted that in the homogeneous phases (SF and NF) there can be only one mode due to one sublattice structure; however, within the reduced Brillouin zone (BZ) we obtain three excitation branches out of which two modes become gapless along the M-K-Γ line due to sublattice symmetry [13,65]. In translation symmetry broken phases (solid and SS) such a degeneracy is lifted except at the K point, and thus they can be identified from the energy gap, say Δ_M at the M point of the BZ for the branches that are degenerate at the K point. For the solid to NF transition, the variation of the energy gap of these two modes at the M point and the density difference $n_{A,B} - n_C$ with increasing temperature are shown in Fig. 4(b). Both quantities undergo a sharp jump at the critical temperature and vanish in the homogeneous NF phase as a consequence of the first-order transition.

Although the collective excitation frequencies both at zero and finite temperatures as well as in the presence of dissipation can be obtained from the linear fluctuation method [24,36,62,63], the effect of quantum and thermal fluctuations on the quasiparticles is beyond the scope of the present study since it requires detailed information on the spectral function $A(\vec{k}, \omega)$ and the dynamic structure factor $S(\vec{k}, \omega)$ [66–69]. It is expected that due to the finite temperature effect, an increase in the width of the above quantities can occur, resulting in a reduction of the excited quasiparticles' lifetime [70–72], which is relevant for its experimental detection. We have also checked that close to zero temperature the excitation spectrum obtained using this method is in agreement with those obtained from spin wave analysis [13]. Although the exact nature and critical behavior of the transition cannot be captured within a simple MF analysis, different phases and the transition between them at finite temperature can be identified from the above-mentioned features of the collective modes and can be relevant for experimental detection. In the next subsection, we consider a cluster of unit cells in order to incorporate the effect of correlation in a systematic way and also discuss how it improves the phase diagram, particularly near $\mu = 3$, where the effect of the geometric frustration of a triangular lattice is much more pronounced and cannot be captured from simple MF theory.
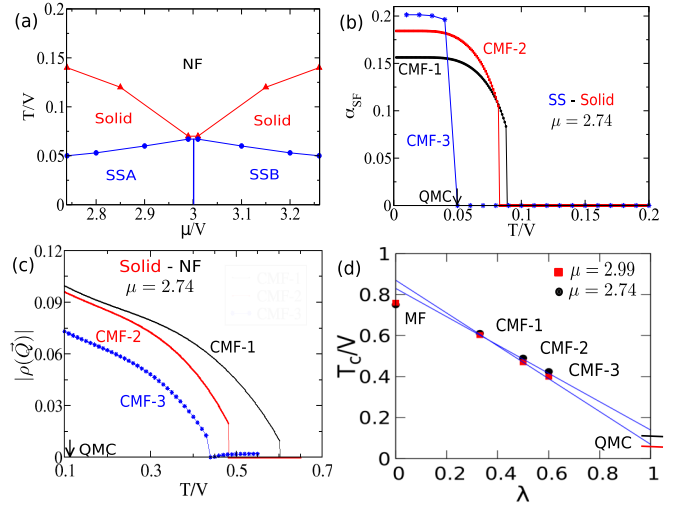

FIG. 5. Finite temperature phase diagram of hardcore bosons in a triangular lattice using CMF: (a) in μ vs T plane for $t = 0.1$. (b), (c) Vanishing of SF order parameter α_{SF} and $\rho(\vec{Q})$ in SS to solid and solid to NF transition, respectively, for different cluster sizes mentioned therein. (d) Infinite cluster size extrapolation of the solid to NF transition temperature (T_c) obtained from the vanishing of $\rho(\vec{Q})$. The extrapolated values are used to obtain the phase diagram in (a) and the phase boundary agrees well with the QMC results [17].

C. Cluster mean field theory

We use the CMF method discussed in Sec. II and investigate the transition temperature between the phases, particularly near $\mu = 3$. Different phases are characterized as follows. The presence of superfluidity is determined by the nonvanishing SF order parameter, $\alpha_{SF} = \sum_{i=1}^{N} \langle \hat{a}_i \rangle / N$, N being the number of lattice sites within the cluster. The density ordering with a two-sublattice structure in DW/solid and SS phase is characterized by a nonvanishing Fourier mode,

$$\rho(\vec{Q}) = \frac{1}{N} \sum_{i=1}^{N} \langle \hat{n}_i \rangle \, e^{i\vec{Q} \cdot \vec{r}_i}, \quad \vec{Q} = (4\pi/3, 0). \quad (14)$$

As a result of two-step melting of the supersolid with increasing temperature, first α_{SF} vanishes, indicating the SS-solid transition, followed by the vanishing of $|\rho(\vec{Q})|$ at higher temperature, showing the solid-NF transition [see Fig. 5(a)]. We observe that the critical temperature, particularly for the solid-NF transition, varies significantly with the cluster size and becomes more and more accurate with increasing size, as depicted in Figs. 5(b) and 5(c). Also, it can be noted that for larger cluster size, the SS-solid transition occurs at much lower temperature compared to that obtained from MF analysis. At this lower temperature, we did not find any trace of SSC phase in between SSA and SSB, resulting in a jump in ρ_{avg} and in α_{SF} across the SSA-SSB boundary. The solid to SS transition caused by lowering the temperature has been predicted to be Berezinskii-Kosterlitz-Thouless (BKT) type [17] due to the absence of long-range order in two dimensions at finite temperature [73]. The algebraic decay of the correlation functions cannot be captured in the present method due to the finite cluster size. However, with increasing cluster size we observe a jump in the SF order parameter α_{SF} at the

SS-solid phase boundary [shown in Fig. 5(b)] resembling the universal jump in the superfluid density at the BKT transition [17]. Moreover, we checked that at the transition, the ratio $T/t\rho_{avg}$ remains nearly the same for different values of μ at a constant interaction strength V. Such a scaling behavior of the transition temperature observed in our study is indicative of the BKT-like transition from solid to SS [74,75].

Further, in order to improve the solid-NF phase boundary, we have performed a finite cluster-size scaling [47] by analyzing the solid-NF transition temperature T_c as a function of a scaling parameter $\lambda = \frac{N_B}{Nz/2}$, where N_B is the number of bonds in a cluster and z is the coordination number, which is 6 for a triangular lattice. The values of T_c obtained from different cluster sizes are plotted as a function of λ in Fig. 5(d). The data are fitted by a straight line and extrapolated to the thermodynamic limit ($\lambda \rightarrow 1$) to extract T_c more accurately. The transition temperature obtained from the quantum Monte Carlo (QMC) study [17] is marked by horizontal cuts. As an example, for $\mu = 2.74$ we obtain that the extrapolated value of T_c/V is 0.14, which is fairly close to the exact value $T_c/V = 0.1033$. Note that such a scaling analysis is different from finite size scaling, which is typically done in the numerical analysis of finite size systems. Similarly, for the same $\mu = 2.74$ the SS-solid transition temperature obtained using a larger cluster is 0.049, which agrees closely with the QMC data $T_c/V = 0.05$ [17]. The resulting phase boundary in the μ versus T plane obtained in this way is shown in Fig. 5(a), which is in very close agreement with the QMC results [17]. Thus our analysis presents how the effect of correlation can be incorporated with increasing order of cluster size, resulting in a remarkable improvement of the phase boundary near $\mu = 3$. However, we do not focus on the type of SS phase formed at $\mu = 3$ [15,17,47], which is beyond the scope of the present study.

IV. PHASES AND COLLECTIVE EXCITATION OF A BOSON WITH FINITE U

In a more realistic scenario concerning the experiment, in this section we discuss the phases and collective modes of bosons with finite on-site interaction U. In addition to the effect of geometric frustration in a triangular lattice, which plays a crucial role in the density ordering of hardcore bosons in terms of boson occupancies in the neighboring sites, in the case of softcore bosons the finite on-site repulsion U competes with NN interaction V as well, and it can affect the boson occupancies in the sublattices. Therefore, our aim is to study the new phases that appear as a result of the combined effect of geometric frustration in a triangular lattice and the interplay between on-site and NN interactions. We focus on the melting of these phases with increasing temperature, and we characterize them from the collective excitation at low temperatures.

A. Zero and finite temperature phases

To this end, we consider the Gutzwiller variational wave function for three sublattices $i =$ A, B, and C, which constitutes the unit cell of a triangular lattice. It is given by

$$|\Psi\rangle = \prod_i |\psi_i\rangle, \quad |\psi_i\rangle = \sum_n f_i^n |n\rangle_i, \quad (15)$$
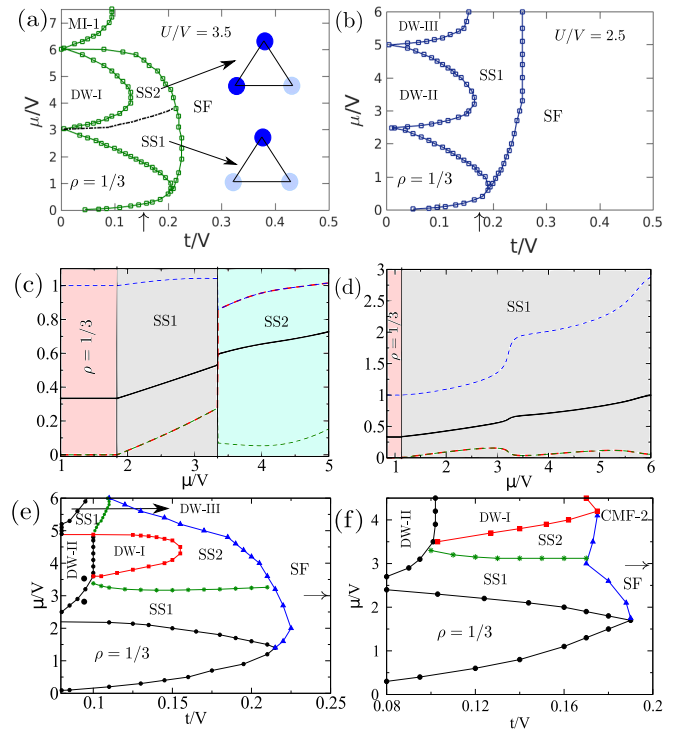

FIG. 6. Zero temperature phase diagram of softcore bosons in a triangular lattice: (a), (b) in μ vs t plane for different values of U/V mentioned therein, (e), (f) for varying on-site interaction $U = 30t$ obtained by using MF and CMF-2, respectively. The schematics in (a) shows the sublattice density configuration in SS1 and SS2. (c), (d) Average density ρ_{avg} (solid line) and sublattice densities $n_{A,B,C}$ (dashed lines) are plotted as a function of μ for $t = 0.15V$, $U = 3.5V$ and for $t = 0.18V$, $U = 2.5V$ corresponding to (a) and (b), respectively.

where $|n\rangle_i$ is the Fock state with occupation number n and probability amplitude $|f_i^n|^2$ at the ith site. In numerical calculation, we do truncation in n suitably with the normalization set to $\sum_n |f_i^n|^2 = 1$. We numerically minimize the energy functional $E = \langle\Psi|\hat{H}_{MF}|\Psi\rangle$ and chart out the phases as a function of μ and t for different values of on-site interaction U in Fig. 6. Since the particle-hole symmetry between $\rho = 1/3$ (1, 0, 0) and DW-I (1,1,0) is destroyed, these insulating lobes are no longer symmetric around $\mu = 3$ [see Fig. 6(a)]. For $U < 3V$, DW phases of higher filling $(n_0, 0, 0)$, $n_0 = 2, 3, \ldots$, e.g., DW-II (2,0,0) and DW-III (3,0,0), appear with increasing μ, as shown in Figs. 6(b) and 6(e). Also, the DW lobe with $\rho = 2/3$ changes from DW-I to DW-II, and MI-1 (1,1,1) becomes DW-III with decreasing U. The continuous deformation of the insulating lobes with decreasing U/V is shown in Appendix B. At finite t, $\rho = 1/3$ and DW-I melts to form two types of supersolids, SS1 and SS2, similar to SSA and SSB phases of hardcore bosons, respectively, for $U > 3V$, whereas below $U = 3V$ only SS1 phase is observed. Such a change in density ordering (also discussed in Appendix B) occurs as a consequence of the interplay between on-site and NN interaction, which can also be viewed as a reduction of geometric frustration due to lowering of U. The sublattice density structures of these supersolids are illustrated in Figs. 6(c) and 6(d) by the dashed lines, as well being schematically depicted
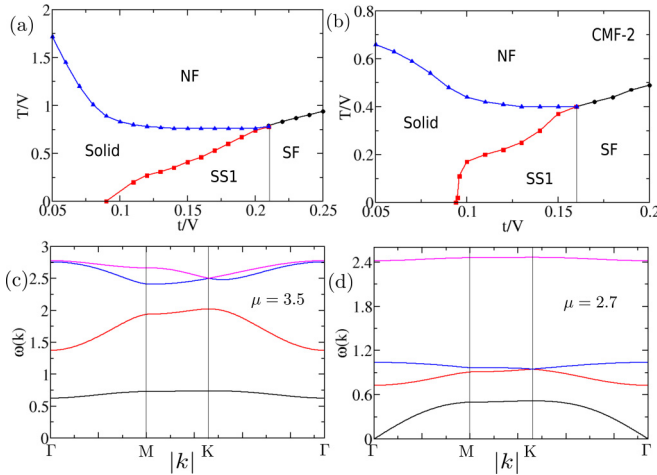
FIG. 7. Finite temperature phase diagram of bosons in a triangular lattice: (a), (b) in t vs T plane for $U = 30t$ and $\mu = 3$ (marked by "$\rightarrow$" on the secondary y-axis in Figs. 6(e) and 6(f), using MF and CMF-2, respectively. (c), (d) Collective excitation of DW-II and SS1 around it, for $\mu = 3.5$ and 2.7, respectively, as marked by (●) in Fig. 6(e), at very low temperature $T = 0.01$.

in Fig. 6(a). We see that the average density [solid line in Fig. 6(c)] exhibits a jump at the SS1-SS2 boundary similar to the hardcore bosons. In Fig. 6(e) we have presented a phase diagram in the μ-t plane with varying U, which scales with respect to t. It can be noted that this simple mean field theory captures all the phases as observed in more exact QMC studies [44], albeit with an expected difference in the phase boundary and an extended SS region over the DW phases. To improve the phase boundary, we incorporate correlation by considering clusters using the zero temperature CMF method described in Sec. II, and the resulting phase diagram is shown in Fig. 6(f).

Next we focus on the melting of the $\rho = 2/3$ lobe as temperature is increased at a fixed chemical potential $\mu = 3$ [marked by "$\rightarrow$" in Figs. 6(e) and 6(f)]. The jump in average density across SS1-SS2 at $T = 0$ is smoothened out at finite temperature, and another type of supersolid is formed between SS1 and SS2, similar to the SSC phase of hardcore bosons. Therefore, we refer the reader to Sec. III A for a similar discussion, and we focus on the thermal melting of the phases such as DW-II and the supersolid SS1 at $\mu = 3$. With increasing T, the supersolid goes through a two-step melting to normal fluid via a solid phase, as depicted in Figs. 7(a) and 7(b). As t/V is increased, the solid region shrinks and thereby the gap between critical temperatures corresponding to the SS-solid and solid-NF transition decreases, and it finally vanishes at the SF-NF boundary. On the other hand, as t/V is decreased, the effect of U starts playing an important role in the melting of DW-II to NF, and the transition temperature increases with increasing V/U as observed from both MF and CMF analysis [see Figs. 7(a) and 7(b)]. However, as expected with decreasing t/V, i.e., in a more correlated regime, the difference between the MF and CMF results of such a transition is more pronounced. It is also important to mention that the SS-SF boundary [the vertical line in Figs. 7(a) and 7(b)] is not affected by the thermal fluctuation, because SF order always vanishes earlier than the DW order with increasing T, thereby

eliminating the possibility of observing the SS-SF transition due to temperature.

B. Collective excitations of softcore bosons

In this section we discuss collective excitation, particularly of the new phases, and we investigate their transitions at finite temperature. To understand the appearance of new stable phases by varying the on-site interaction U, we first consider the excitations of insulating phases at zero temperature and for vanishing hopping strength. For sufficiently large on-site repulsion U, similar density ordering to that of hardcore bosons occurs, and DW phases can be classified as $(n_0, n_0 - 1, n_0 - 1)$ and $(n_0, n_0, n_0 - 1)$ representing the number of particles at sublattice (A, B, C), respectively. First the (1,0,0) DW phase appears, which has two degenerate particle excitations at A, B sites with energy $E_p^{A,B} = 3V - \mu$ and particle (hole) excitation energy $E_p^C = U - \mu$ ($E_h^C = \mu$) at site C. The hole excitation E_h^C becomes unstable at $\mu = 0$, and for large U the instability of particle excitation E_p^A at $\mu = 3V$ leads to the formation of DW-I with filling $2/3$. However, this scenario changes for $U < 3V$ when the particle excitation E_p^C at C becomes unstable first at $\mu = U < 3V$ and a new DW-II phase appears. In Fig. 6(b) note that these are boundary points of $\rho = 1/3$ phase in the atomic limit ($t = 0$). In DW-I the low-lying modes are degenerate hole excitations $E_h^{A,B} = \mu - 3V$ and particle excitation $E_p^C = 6V - \mu$, which become unstable at $\mu = 3V$ and $6V$, respectively. For large U these low-lying modes are similar to those of hardcore bosons, and we skip that discussion. Instead we focus on the $U < 3V$ regime and the DW-II phase, which has degenerate particle excitation $E_p^{A,B} = 6V - \mu$ and two lower energy particle (hole) excitation $E_p^C = 2U - \mu$ ($E_h^C = \mu - U$). These determine the stability of this phase within the region $U < \mu < 2U$ [note that these are the boundaries of DW-II for $t = 0$ in Fig. 6(b)]. For finite t, its low-lying excitations are shown in Fig. 7(c). Unlike the hardcore bosons, at finite U the dimension of the Fock space at each site is infinite in principle; however, for numerical calculation we truncate at a finite maximum boson occupancy as required, and we plot a few low-lying energy modes, but we exclude the higher excitation branches, which are not relevant in our study. As t is increased, DW-II melts to SS1 phase along with the vanishing of the Mott energy gap at the Γ point. The low-lying excitation of SS1 surrounding DW-II is shown in Fig. 7(d). The lowest energy branch represents the gapless sound mode, which can be identified as the Goldstone mode. The energy gap of the next excitation branch at $|k| \sim 0$ gradually decreases with decreasing t and exhibits a dip near the transition from SS1 to DW-II phase, resembling the behavior of the Higgs-like massive mode [76–78]. The gap between the lowest two branches of excitation at the K point vanishes for $U > 3V$, reminiscent of the lowest degenerate hole excitation of DW (1,1,0) [see Fig. 3(b)]. This completes our analysis on the characteristic features of the excitation of new phases at finite U and low temperature.

V. SUMMARY

To summarize, we studied various phases of bosons and their collective excitations in a triangular lattice at finite

temperature both for on-site hardcore repulsion ($U \to \infty$) and for finite U. The effect of lattice geometric frustration and strong correlation between the atoms plays a crucial role in the formation of different phases and transition between them. We obtained a finite temperature phase diagram using a single-site mean field method approximating the density matrix as a product of single-site density matrices and thereby ignoring the intersite correlation. The main advantage of doing MF is to obtain a semianalytic estimate of the phase boundaries within the framework of Landau theory, particularly for hardcore bosons. We also performed more accurate cluster mean field theory and compare the results of both in order to gain information about the effect of correlation. Moreover, the collective excitation frequencies of the various phases at finite temperature are calculated from the time dependent fluctuations of the density matrix. Different characteristics of such low-lying excitations carry the signature of various phases and signals the transition between them, which can be used for their experimental detection.

As a result of the interplay between geometric frustration in a triangular lattice and nearest neighbor as well as on-site boson repulsion, a stable supersolid phase is formed around the DW phases with different filling (depending on μ and U). With increasing temperature, two-step melting of the SS phase is observed; first, the SF order parameter vanishes at much lower temperature, which scales with hopping strength, and then the solid phase melts to homogeneous NF at higher temperature comparable with nearest neighbor interaction. As t/V increases, the gap between these two transition temperatures eventually vanishes and merges to the SF-NF phase boundary. Within MF theory we observe a continuous transition between SS-DW/solid and SF-NF phases. The gapless sound mode at $k = 0$ present in SF and SS phases becomes gapped at their respective phase boundaries, whereas the solid phase undergoes a first-order transition to NF with increasing T, characterized by a jump in DW order parameters such as sublattice density imbalance δ and Fourier mode $\rho(\vec{Q})$ at $\vec{Q} = (4\pi/3, 0)$. The degenerate excitation modes of the DW phase at the K point also become gapless at the M point of the Brillouin zone during the transition to homogeneous NF. The behavior of the collective excitation of different phases at finite T is important in the context of recent cold atom experiments where the low energy Goldstone and Higgs modes in a supersolid are detected using spectroscopic measurement [40] or using the time-of-flight experiments [41–43].

Although simple MF theory provides a qualitative understanding of the finite temperature phases, as expected it fails to capture the exact nature of the transition as well as the quantitative estimate of the transition temperature, particularly the melting of SS and solid phases due to the effect of frustration. For hardcore bosons at and around $\mu = 3$, the enhanced effect of frustration significantly reduces the melting temperature of the DW phase. For $t = 0$ the system of hardcore bosons becomes equivalent to a disordered antiferromagnet with vanishing critical temperature. By incorporating finite cluster-size scaling, CMFT can successfully capture such a reduction of the melting temperature around $\mu = 3$, which is also in agreement with the QMC results [17,44]. This indicates that the effects of both correlation and frustration can be captured by CMFT, which is thus a useful tool to

study the finite temperature phases of interacting bosons in an optical lattice and phase transitions between them. Such a method can be extended further to study the nonequilibrium dynamics of strongly correlated lattice bosons at finite temperature.

In conclusion, we have investigated the effect of correlation arising from geometric frustration in a triangular lattice and interaction systematically using mean field as well as cluster mean field theory, and we identified the different phases from their characteristic low-lying excitation. These collective modes and their behavior at finite temperature that we discussed can be probed experimentally using a similar line of thought to that in recent cold atom setups [40–43].

APPENDIX A: LANDAU-GINZBURG THEORY OF PHASE TRANSITION

In the following subsections, we will discuss in detail the estimation of the transition temperature, and the nature of the transition between different phases from the LG theory.

1. Superfluid to normal fluid transition

In the homogeneous SF phase, the average free energy of the system given in Eq. (6) can be written as

$$F = -6t\alpha^2 - \frac{\mu}{2}(1+m) + \frac{3V}{4}(1+m)^2 + T\sum_{\sigma=+,-}\lambda_\sigma \ln\lambda_\sigma,$$
(A1)

where $\lambda_\pm = (1 \pm \sqrt{m^2 + 4\alpha^2})/2$. We have assumed α to be a real parameter without any loss of generality, and because of homogeneity of the superfluid we have set $\alpha_i = \alpha$ and $m_i = m$. Now the free energy can be expanded in a power series of SF order parameter α as follows:

$$F = a(\mu, t, m, T) + b(\mu, t, m, T)\alpha^2 + c(\mu, t, m, T)\alpha^4 + \cdots.$$
(A2)

This is the Landau-Ginzburg form of the second-order phase transition. Thus the critical temperature can be estimated by numerically finding the values of m and then evaluating the coefficients a, b, c of Eq. (A2). In Fig. 8(a) we have plotted F at $T < T_c$, $T = T_c$, and $T > T_c$.

As mentioned in the main text, we observe that with increasing temperature the SF order parameter vanishes continuously at the SF-NF phase boundary. In Fig. 8(b) we have shown the variation of the SF order parameter as a function of temperature. It can be noted that the numerically obtained value of the critical temperature [as marked by $\uparrow$ in Fig. 8(b)] agrees with that estimated from the LG theory.

2. Solid to normal fluid transition

The density wave phase is characterized by vanishing of SF order parameters ($\alpha = 0$) and a nonzero value of
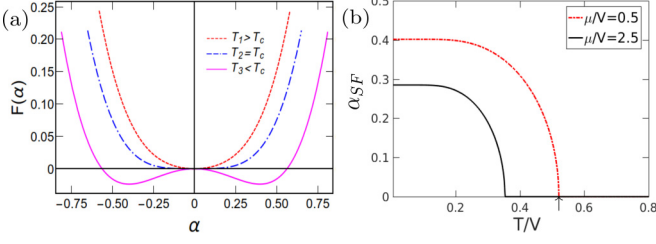
FIG. 8. (a) Landau free energy F as a function of the average SF order parameter $\alpha_{SF} = \alpha$ for different T, each of them scaled by subtracting $F(\alpha = 0)$. Parameters are $t/V = 0.2$ and $\mu/V = 0.5$. (b) α_{SF} with increasing temperature at $t/V = 0.2$ for different μ/V as mentioned in the inset. The numerically obtained SF-NF transition temperature T_c agrees with that from the LG theory as marked by ($\uparrow$) on the T/V axis.

density order ($m_i \neq m_{\bar{i}}$). Let us consider $n_A = n_B = (n - \delta)$ and $n_C = (n + 2\delta)$, where δ is the DW order parameter. Following this parametrization, the free energy in terms of m and δ is given by

$$F = \frac{3V}{4}(m^2 + 2m - 4\delta^2 + 1) - \frac{\mu}{2}(1 + m)$$
$$+ \frac{T}{3} \sum_{\substack{i = A, B, C \\ j = 1, 2}} \lambda_i^j \ln \lambda_i^j, \tag{A3}$$

where $\lambda_A^{1,2} = \lambda_B^{1,2} = [1 \pm (m - 2\delta)]/2$ and $\lambda_C^{1,2} = [1 \pm (m + 4\delta)]/2$. For a given value of m, we can write the free energy in a power series of δ, which is given by

$$F = a(\mu, t, m, T) + b(\mu, t, m, T)\delta + c(\mu, t, m, T)\delta^2$$
$$+ d(\mu, t, m, T)\delta^3 + \cdots. \tag{A4}$$

Nonzero values of the coefficients of odd powers in δ, e.g., d, imply that this is the Landau-Ginzburg form of the first-order phase transition. The critical temperature can be obtained by evaluating the coefficients a, b, c, d by numerically finding the value of m.

In Fig. 9(a) we have shown the typical variation of LG free energy as a function of δ. At the critical T_c, δ corresponding to the minima of F exhibits a jump from a finite value to zero as depicted in Fig. 9(c). Such a jump is a characteristic feature of the first-order transition from solid to NF phase. However, the magnitude of the jump reduces as μ/V becomes closer to 3 and vanishes at $\mu = 3$ as shown in Fig. 9(d). We would like to point out that a similar phenomenon was observed in the case of the SS to SF phase transition at zero temperature [47]. The average density ρ_{avg}, the sublattice density imbalance δ, and its jump Δ at the solid-NF phase boundary behave symmetrically away from $\mu/V = 3$, as can be noted from Figs. 9(b), 9(c), and 9(d), respectively.

APPENDIX B: ZERO TEMPERATURE PHASE DIAGRAM OF SOFTCORE BOSONS

Here we show how the breaking of particle hole symmetry due to finite U deforms the insulating lobes, and new
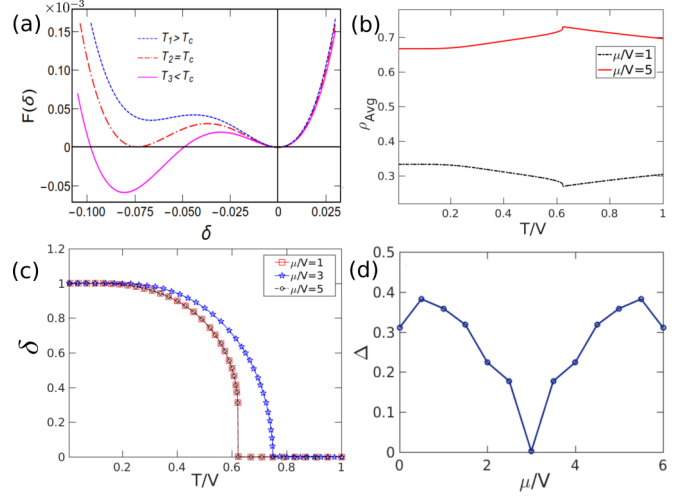

FIG. 9. (a) Landau free energy F is plotted as a function of δ, scaled by subtracting $F(\delta = 0)$ for $\mu/V = 5$ and for different temperatures mentioned therein. (b), (c) Average density ρ_{avg} and sublattice density imbalance δ with increasing T for different μ/V. (d) Magnitude of the jump Δ in δ at T_c for solid-NF transition vs μ/V. We set $t/V = 0$.

density wave phases with higher filling appear. In Fig. 10 we have demonstrated this issue, where U is gradually decreased from a large value for which we recover the hardcore boson phase diagram. For $U > 3V$, we observe density waves $\rho = 1/3$ $(1, 0, 0)$, DW-I $(1,1,0)$, Mott insulators MI-1 $(1,1,1)$, and so on with increasing μ. Melting of $\rho = 1/3$ and DW-I $(1,1,0)$ gives rise to the formation of SS1 and SS2 supersolids, similar to SSA and SSB phases for hardcore bosons (as discussed in Sec. IV A). With decreasing U these insulating lobes deform, and below $U = 3V$, the $\rho = 2/3$ phase changes from $(1,1,0)$ to $(2,0,0)$ along with the appearance of other DW phases with higher filling, such as DW-III $(3,0,0)$, DW-IV $(4,0,0)$, and so on, as μ is increased. Also, an extended supersolid of type SS1 forms above these insulating phases. The sublattice density structures of these supersolids are shown in Fig. 6(a).
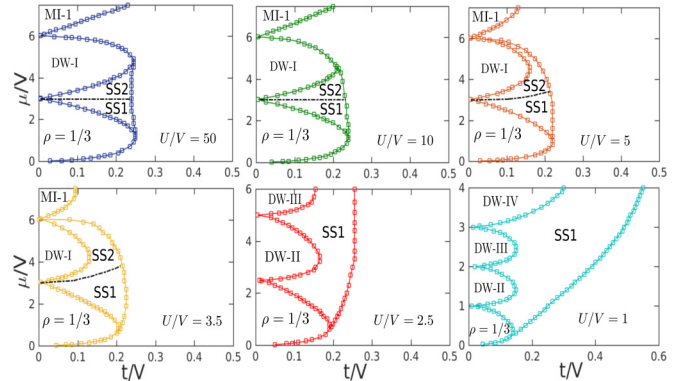

FIG. 10. Zero temperature mean field phase diagram of bosons with finite U in the μ-t plane. Different values of U are mentioned in the inset.

[1] C. Lacroix, P. Mendels, and F. Mila, *Introduction to Frustrated Magnetism: Materials, Experiments, Theory* (Springer, New York, 2011), Vol. 164

[2] L. Balents, Nature (London) **464**, 199 (2010).

[3] M. J. Harris, S. T. Bramwell, D. F. McMorrow, T. Zeiske, and K. W. Godfrey, Phys. Rev. Lett. **79**, 2554 (1997).

[4] S. T. Bramwell and M. J. P. Gingras, Science **294**, 1495 (2001).

[5] G. H. Wannier, Phys. Rev. **79**, 357 (1950).

[6] T. Fennell, P. P. Deen, A. R. Wildes, K. Schmalzl, D. Prabhakaran, A. T. Boothroyd, R. J. Aldus, D. F. McMorrow, and S. T. Bramwell, Science **326**, 415 (2009).

[7] Y. Shirata, H. Tanaka, A. Matsuo, and K. Kindo, Phys. Rev. Lett. **108**, 057205 (2012).

[8] T. Susuki, N. Kurita, T. Tanaka, H. Nojiri, A. Matsuo, K. Kindo, and H. Tanaka, Phys. Rev. Lett. **110**, 267201 (2013).

[9] Y. Shen *et al.*, Nature (London) **540**, 559 (2016).

[10] C. Becker, P. Soltan-Panahi, J. Kronjäger, S. Dörscher, K. Bongs, and K. Sengstock, New J. Phys. **12**, 065025 (2010).

[11] J. Struck, C. Ölschläger, R. Le Targat, P. Soltan-Panahi, A. Eckardt, M. Lewenstein, P. Windpassinger, and K. Sengstock, Science **333**, 996 (2011).

[12] J. Struck, M. Weinberg, C. Ölschläger, P. Windpassinger, J. Simonet, K. Sengstock, R. Höppner, P. Hauke, A. Eckardt, M. Lewenstein, and L. Mathey, Nat. Phys. **9**, 738 (2013).

[13] G. Murthy, D. Arovas, and A. Auerbach, Phys. Rev. B **55**, 3104 (1997).

[14] S. Wessel and M. Troyer, Phys. Rev. Lett. **95**, 127205 (2005).

[15] D. Heidarian and K. Damle, Phys. Rev. Lett. **95**, 127206 (2005).

[16] R. G. Melko, A. Paramekanti, A. A. Burkov, A. Vishwanath, D. N. Sheng, and L. Balents, Phys. Rev. Lett. **95**, 127207 (2005).

[17] M. Boninsegni and N. Prokof'ev, Phys. Rev. Lett. **95**, 237204 (2005).

[18] A. F. Andreev and I. M. Lifshitz, Sov. Phys. JETP **29**, 1107 (1969); G. V. Chester, Phys. Rev. A **2**, 256 (1970).

[19] A. J. Leggett, Phys. Rev. Lett. **25**, 1543 (1970); Science **305**, 1921 (2004).

[20] M. Boninsegni and N. V. Prokof'ev, Rev. Mod. Phys. **84**, 759 (2012); N. Prokof'ev, Adv. Phys. **56**, 381 (2007).

[21] H. Matsuda and T. Tsuneto, Prog. Theor. Phys. Suppl. **46**, 411 (1970); K. S. Liu and M. E. Fisher, J. Low Temp. Phys. **10**, 655 (1972).

[22] G. G. Batrouni, R. T. Scalettar, G. T. Zimanyi, and A. P. Kampf, Phys. Rev. Lett. **74**, 2527 (1995); R. T. Scalettar, G. G. Batrouni, A. P. Kampf, and G. T. Zimanyi, Phys. Rev. B **51**, 8467 (1995).

[23] V. W. Scarola and S. Das Sarma, Phys. Rev. Lett. **95**, 033003 (2005); V. W. Scarola, E. Demler, and S. Das Sarma, Phys. Rev. A **73**, 051601(R) (2006).

[24] D. L. Kovrizhin, G. V. Pai, and S. Sinha, Europhys. Lett. **72**, 162 (2005).

[25] P. Sengupta, L. P. Pryadko, F. Alet, M. Troyer, and G. Schmid, Phys. Rev. Lett. **94**, 207202 (2005).

[26] D. Yamamoto, A. Masaki, and I. Danshita, Phys. Rev. B **86**, 054516 (2012); S. Bandyopadhyay, R. Bai, S. Pal, K. Suthar, R. Nath, and D. Angom, Phys. Rev. A **100**, 053623 (2019).

[27] A. van Otterlo, K. H. Wagenblast, R. Baltin, C. Bruder, R. Fazio, and G. Schön, Phys. Rev. B **52**, 16176 (1995).

[28] E. Roddick and D. Stroud, Phys. Rev. B **51**, 8672(R) (1995).

[29] H. P. Büchler and G. Blatter, Phys. Rev. Lett. **91**, 130404 (2003).

[30] I. Titvinidze, M. Snoek, and W. Hofstetter, Phys. Rev. Lett. **100**, 100401 (2008); Phys. Rev. B **79**, 144506 (2009).

[31] S. Sinha and K. Sengupta, Phys. Rev. B **79**, 115124 (2009); P. P. Orth, D. L. Bergman, and K. Le Hur, Phys. Rev. A **80**, 023624 (2009).

[32] S. Giovanazzi, D. O'Dell, and G. Kurizki, Phys. Rev. Lett. **88**, 130402 (2002).

[33] K. Góral, L. Santos, and M. Lewenstein, Phys. Rev. Lett. **88**, 170406 (2002).

[34] Y. Li, L. P. Pitaevskii, and S. Stringari, Phys. Rev. Lett. **108**, 225301 (2012).

[35] N. Henkel, R. Nath, and T. Pohl, Phys. Rev. Lett. **104**, 195302 (2010).

[36] K. Saha, S. Sinha, and K. Sengupta, Phys. Rev. A **89**, 023618 (2014).

[37] A. Geißler, U. Bissbort, and W. Hofstetter, Phys. Rev. A **98**, 063635 (2018).

[38] J. R. Li, J. Lee, W. Huang, S. Burchesky, B. Shteynas, F. C. Top, A. O. Jamison, and W. Ketterle, Nature (London) **543**, 91 (2017).

[39] R. Landig, L. Hruby, N. Dogra, M. Landini, R. Mottl, T. Donner, and T. Esslinger, Nature (London) **532**, 476 (2016).

[40] J. Léonard, A. Morales, P. Zupancic, T. Donner, and T. Esslinger, Science **358**, 1415 (2017).

[41] G. Natale, R. M. W. van Bijnen, A. Patscheider, D. Petter, M. J. Mark, L. Chomaz, and F. Ferlaino, Phys. Rev. Lett. **123**, 050402 (2019).

[42] M. Guo, F. Böttcher, J. Hertkorn, J. N. Schmidt, M. Wenzel, H. P. Büchler, T. Langen, and T. Pfau, Nature (London) **574**, 386 (2019).

[43] L. Tanzi, S. M. Roccuzzo, E. Lucioni, F. Famá, A. Fioretti, C. Gabbanini, G. Modugno, A. Recati, and S. Stringari, Nature (London) **574**, 382 (2019).

[44] J. Y. Gan, Y. C. Wen, and Y. Yu, Phys. Rev. B **75**, 094501 (2007).

[45] F. Wang, F. Pollmann, and A. Vishwanath, Phys. Rev. Lett. **102**, 017203 (2009).

[46] L. Pollet, J. D. Picon, H. P. Büchler, and M. Troyer, Phys. Rev. Lett. **104**, 125302 (2010).

[47] D. Yamamoto, I. Danshita, and C. A. R. Sá de Melo, Phys. Rev. A **85**, 021601(R) (2012).

[48] X. F. Zhang, S. Hu, A. Pelster, and S. Eggert, Phys. Rev. Lett. **117**, 193201 (2016).

[49] J. Panas, M. Barbier, A. Geißler, and W. Hofstetter, Phys. Rev. A **99**, 063625 (2019).

[50] B. Capogrosso-Sansone, S. G. Söyler, N. Prokof'ev, and B. Svistunov, Phys. Rev. A **77**, 015602 (2008); B. Capogrosso-Sansone, N. V. Prokof'ev, and B. V. Svistunov, Phys. Rev. B **75**, 134302 (2007).

[51] A. S. Sajna, T. P. Polak, R. Micnas, and P. Rozek, Phys. Rev. A **92**, 013602 (2015).

[52] K. W. Mahmud, E. N. Duchon, Y. Kato, N. Kawashima, R. T. Scalettar, and N. Trivedi, Phys. Rev. B **84**, 054302 (2011).

[53] M. Kübler, F. T. Sant'Ana, F. E. A. Santos, and A. Pelster, Phys. Rev. A **99**, 063603 (2019); F. T. Sant'Ana, A. Pelster, and Francisco Ednilson Alves dos Santos, *ibid.* **100**, 043609 (2019).

[54] A. Joshi and P. Majumdar, Eur. Phys. J. B **93**, 33 (2020).

[55] D. Pekker, B. Wunsch, T. Kitagawa, E. Manousakis, A. S. Sørensen, and E. Demler, Phys. Rev. B **86**, 144527 (2012); D.-S. Lühmann, Phys. Rev. A **87**, 043619 (2013).

[56] M. Singh, T. Mishra, R. V. Pai, and B. P. Das, Phys. Rev. A **90**, 013625 (2014); S. Pal, R. Bai, S. Bandyopadhyay, K. Suthar, and D. Angom, *ibid.* **99**, 053610 (2019).

[57] J. Jin, A. Biella, O. Viyuela, L. Mazza, J. Keeling, R. Fazio, and D. Rossini, Phys. Rev. X **6**, 031011 (2016); G. Piccitto, B. Zunkovic, and A. Silva, Phys. Rev. B **100**, 180402(R) (2019).

[58] S. Alexander, Phys. Lett. **54A**, 353 (1975).

[59] R. M. F. Houtappel, Physica **16**, 425 (1950).

[60] K. Husimi and I. Syozi, Prog. Theor. Phys. **5**, 341 (1950).

[61] M. Schick, J. S. Walker, and M. Wortis, Phys. Rev. B **16**, 2205 (1977); P. A. Slotte, J. Phys. A **17**, L85 (1984).

[62] D. L. Kovrizhin, G. V. Pai, and S. Sinha, arXiv:0707.2937.

[63] S. Ray, S. Sinha, and K. Sengupta, Phys. Rev. A **93**, 033627 (2016).

[64] S. A. Owerre, Phys. Rev. B **93**, 094436 (2016).

[65] T. Baghdasaryan, T. Geernaert, K. Chah, C. Caucheteur, K. Schuster, J. Kobelke, H. Thienpont, and F. Berghmans, Sci. Rep. **8**, 5470 (2018).

[66] P. Coleman, *Introduction to Many-Body Physics* (Cambridge University Press, Cambridge, 2015).

[67] S. Stringari, Phys. Rev. B **46**, 2974 (1992).

[68] P. Pippan, H. G. Evertz, and M. Hohenadler, Phys. Rev. A **80**, 033612 (2009).

[69] J. Panas, A. Kauch, J. Kunes, D. Vollhardt, and K. Byczuk, Phys. Rev. B **92**, 045102 (2015).

[70] T. L. Dao, A. Georges, J. Dalibard, C. Salomon, and I. Carusotto, Phys. Rev. Lett. **98**, 240402 (2007).

[71] M. D. Reichl and E. J. Mueller, Phys. Rev. A **91**, 043627 (2015).

[72] R. Landig, F. Brennecke, R. Mottl, T. Donner, and T. Esslinger, Nat. Commun. **6**, 7046 (2015).

[73] P. C. Hohenberg, Phys. Rev. **158**, 383 (1967); N. D. Mermin and H. Wagner, Phys. Rev. Lett. **17**, 1133 (1966).

[74] N. Prokof'ev, O. Ruebenacker, and B. Svistunov, Phys. Rev. Lett. **87**, 270402 (2001).

[75] M. Holzmann, G. Baym, J.-P. Blaizot, and F. Laloë, Proc. Natl. Acad. Sci. USA **104**, 1476 (2007).

[76] D. Pekker and C. M. Varma, Annu. Rev. Condens. Matter Phys. **6**, 269 (2015).

[77] L. Pollet and N. Prokof'ev, Phys. Rev. Lett. **109**, 010401 (2012).

[78] D. Podolsky, A. Auerbach, and D. P. Arovas, Phys. Rev. B **84**, 174522 (2011); S. Gazit, D. Podolsky, and A. Auerbach, Phys. Rev. Lett. **110**, 140401 (2013).